CANCER

Immune activation is essential for the antitumor activity of EZH2 inhibition in urothelial carcinoma

Andrea Piunti[1,2,3]*, Khyati Meghani[3,4], Yanni Yu[3,4], A. Gordon Robertson[5], Joseph R. Podojil[6], Kimberly A. McLaughlin[3,4], Zonghao You[3,4], Damiano Fantini[3,4], MingYi Chiang[6], Yi Luo[7], Lu Wang[3], Nathan Heyen[3,4,5], Jun Qian[3,4,8], Stephen D. Miller[6], Ali Shilatifard[3], Joshua J. Meeks[3,4,8]*

The long-term survival of patients with advanced urothelial carcinoma (UCa) is limited because of innate resistance to treatment. We identified elevated expression of the histone methyltransferase EZH2 as a hallmark of aggressive UCa and hypothesized that EZH2 inhibition, via a small-molecule catalytic inhibitor, might have antitumor effects in UCa. Here, in a carcinogen-induced mouse bladder cancer model, a reduction in tumor progression and an increase in immune infiltration upon EZH2 inhibition were observed. Treatment of mice with EZH2i causes an increase in MHC class II expression in the urothelium and can activate infiltrating T cells. Unexpectedly, we found that the lack of an intact adaptive immune system completely abolishes the antitumor effects induced by EZH2 catalytic inhibition. These findings show that immune evasion is the only important determinant for the efficacy of EZH2 catalytic inhibition treatment in a UCa model.

INTRODUCTION

Urothelial carcinoma (UCa) is the fifth most common cancer in the United States with more than 81,000 annual incident diagnoses (*1*). Across all stages of UCa, resistance to immunotherapy results in recurrence and progression and is ultimately the cause of mortality for most patients (*2*). Multiple mechanisms of immune resistance have been described in UCa, including loss of neoantigens, suppression of T cell–mediated activity by myeloid and regulatory cells, and immune exhaustion (*3*–*5*). Therefore, immunotherapy strategies in UCa have involved reactivation of a suppressed immune response. In high-risk non–muscle invasive bladder cancer (NMIBC), for example, intravesical immunotherapy using a latent form of tuberculosis vaccine [Bacillus Calmette-Guérin (BCG)] induces both BCG-directed and tumor-specific immunity, ultimately decreasing recurrence and progression (*2*, *6*–*9*). If BCG is ineffective, a second line option is the Programmed cell death protein 1 (PD-1) inhibitor, pembrolizumab, found to decrease recurrence by 25% at 12 months (*10*). In the advanced setting, monotherapy with PD1/programmed death ligand 1 inhibitors is both a first- and second-line therapy for patients with metastatic UCa, but only 30% of patients achieve a durable response of more than 12 months, presumably due to innate resistance (*11*, *12*). Therefore, chemotherapy remains the first-line treatment for metastatic UCa because immunotherapy is only half as effective as chemotherapy to achieve an initial objective response (23% versus 47%). Yet, immunotherapy "responsive" tumors achieve long-term remission (median duration of 8.5 months for chemotherapy versus not achieved for atezolizumab in IMvigor130) (*13*). It remains unknown if this resistance is from tumor-mediated immune suppression, insufficient immune activation or inadequate antigen presentation, and recognition of the tumor by the host immune microenvironment.

Recently, we identified a subtype of high-risk NMIBCs that had elevated expression of E2F and EZH2 (enhancer of zeste homolog 2), suppression of immune-related signatures, and was associated with a high frequency of carcinoma in situ (T1-LumGU) (*14*). Previously, high EZH2 expression was also found in muscle invasive bladder cancer (MIBC) and correlated with a shorter time to recurrence (*15*, *16*). EZH2 is the catalytic subunit of the polycomb repressive complex 2 (PRC2), a multiprotein histone methyltransferase complex targeting lysine-27 on histone H3 (H3K27) and generally involved in transcriptional repression (*17*, *18*). EZH2 is frequently dysregulated in cancer and regarded as an oncogene across different tumor types (*19*, *20*). Small-molecule catalytic inhibitors targeting EZH2 activity have been developed, and one in particular, tazemetostat, has been recently approved by the U.S. Food and Drug Administration for the treatment of epithelioid sarcoma and relapsed/refractory follicular lymphoma. The function of EZH2 in cancer is well established and is generally considered to regulate aberrant proliferation, invasion, and other hallmarks of cancers (*21*, *22*). EZH2 catalytic inhibition has shown efficacy in xenograft UCa models with loss of KDM6A activity by affecting cancer cell growth through a cell autonomous mechanism (*23*).

In this study, we explore the role of EZH2 activity in an immunocompetent carcinogen-induced UCa mouse model that faithfully recapitulates features of human UCa (*24*). Unexpectedly, we not only find that this UCa model is sensitive to EZH2 catalytic inhibition, but we also demonstrate that this antitumor activity is completely dependent on an intact adaptive immune system. These results support a previously unidentified immunomodulatory role for EZH2 in promoting UCa in a non–cell autonomous manner, paving the way for potential combination therapies with immune checkpoint inhibitors.

[1]Division of Hematology/Oncology, Department of Pediatrics, University of Chicago, Chicago, IL, USA. [2]University of Chicago Medicine Comprehensive Cancer Center, Chicago, IL, USA. [3]Department of Biochemistry and Molecular Genetics, Simpson Querrey Institute for Epigenetics, Northwestern University Feinberg School of Medicine, Chicago, IL, USA. [4]Department of Urology, Feinberg School of Medicine, Chicago, IL, USA. [5]Dxige Research Inc., Courtenay, BC, Canada. [6]Department of Microbiology and Immunology, Feinberg School of Medicine, Chicago, IL, USA. [7]Department of Urology, University of Iowa, Iowa City, IA, USA. [8]Jesse Brown VA Medical Center, Chicago, IL, USA.
*Corresponding author. Email: joshua.meeks@northwestern.edu (J.J.M.); piunti@uchicago.edu (A.P.)

RESULTS

Ezh2 catalytic targeting inhibits tumor progression in a carcinogen-induced MIBC model

Similar to many other malignancies, EZH2 is overexpressed in bladder cancer (BCa) compared to normal tissue along with increased levels of repressive H3K27me3 (Fig. 1A) (*16*). The increase in EZH2 expression in tumor cells is often due to aberrant transcriptional regulation of the gene. This is associated to the deregulated activity of the pRB (Retinoblastoma)–E2F pathway that is often affected in BCa (*14*, *25*). Our group has previously characterized the BBN [*N*-butyl-*N*-(4-hydroxybutyl) nitrosamine] carcinogen-induced mouse model of MIBC and found that the mutation landscape of tumors observed in mice upon BBN exposure is similar to human BCa (*24*, *26*). BBN exposure time correlates with more homogeneously aggressive histopathology (*27*). Using this model, we recapitulated the time-dependent increase of *Ezh2* expression upon treatment with the BBN carcinogen that correlates with the development of MIBC in our mouse model (Fig. 1B).

Next, we were interested in evaluating, using a genetic approach, the relevance of Ezh2 expression for disease progression in our MIBC

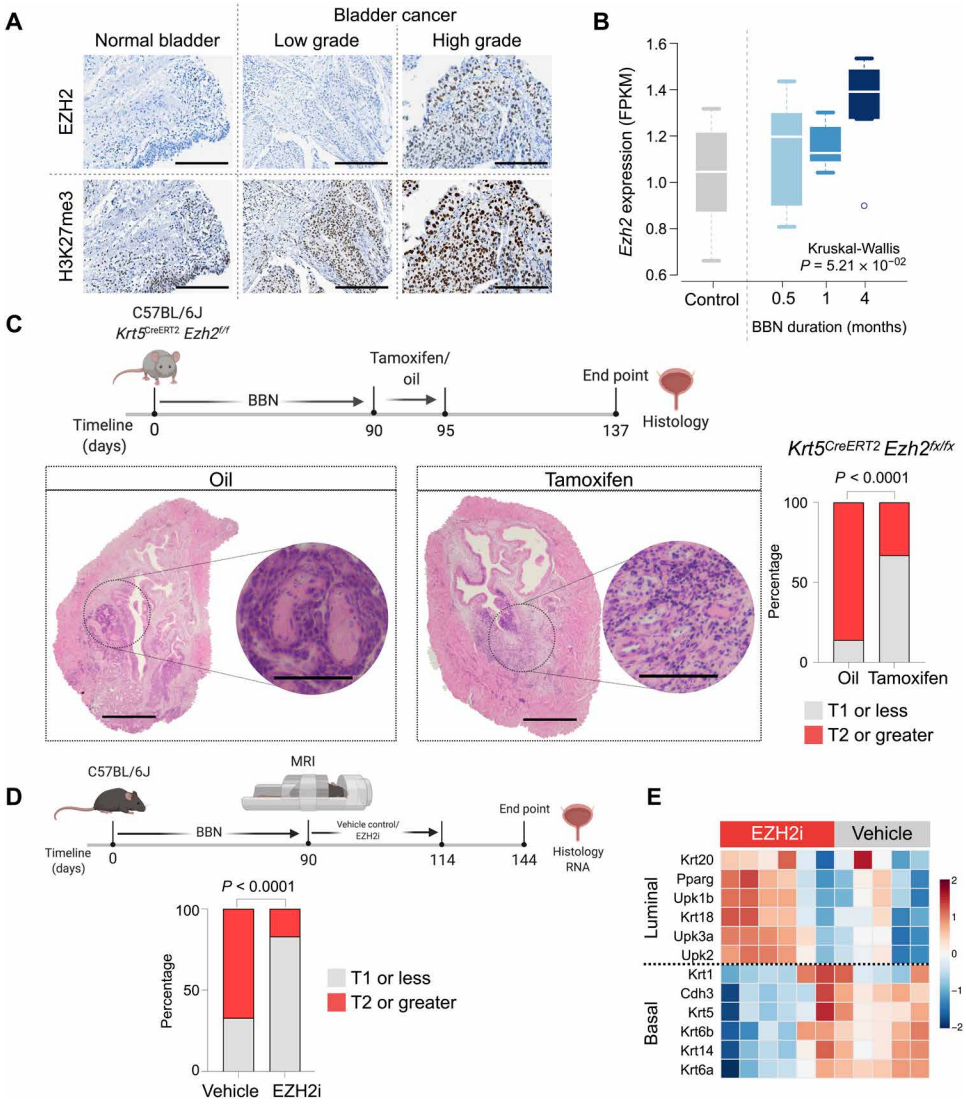

Fig. 1. EZH2 and its catalytic function promote higher BCa stages. (**A**) Immunohistochemistry of human tumors and normal bladder for EZH2 and H3K27me3 in normal, low-grade, and high-grade BCa. Scale bars, 200 μM. (**B**) *Ezh2* expression in bladders from mice administered with *N*-butyl-*N*-(4-hydroxybutyl) nitrosamine (BBN) carcinogen for different durations. FPKM, fragments per kilobase of transcript per million mapped reads. (**C**) Schematic describing the experimental design for evaluating the role of *Ezh2* in BBN-mediated tumor progression. Left: Representative immunohistochemistry sections of BBN tumors from $Krt5^{CreERT2}$ $Ezh2^{f/f}$ mice treated with oil control or tamoxifen. Inset pictures show representative histology of the selected areas. Scale bars, 1 mm (whole bladder) and 100 μm (highlighted section). Right: Quantification of tumor stage in mice from indicated conditions. (**D** and **E**) Male C57BL/6 mice received water containing 0.05% BBN for 90 days, after which the presence of a tumor was confirmed using magnetic resonance imaging (MRI), and mice were treated with vehicle control ($n = 9$) or EPZ011989 ($n = 12$) for 24 days. One month after treatment, animals were euthanized for analysis. (D) Schematic describing the experimental design for evaluating the efficacy of EZH2i in carcinogen-induced tumor model. Mice treated with EZH2i had fewer high-grade tumors (stage T2 or higher) compared to vehicle control. (E) Analysis of mRNA expression levels of different phenotypic markers demonstrates reversion of EZH2i-treated tumors to a more luminal state compared to the more basal markers observed in the vehicle control–treated tumors.

mouse model. Therefore, we generated a conditional mouse model where the *Ezh2* gene would be deleted specifically in basal epithelial cells, including those from the urothelium that are plausibly the cells of origin for MIBC (*27*). To obtain this model, we crossed *Krt5-Cre-ER*^{T2} mice with *Ezh2*$^{fx/fx}$ mice to generate *Krt5-Cre-ER*^{T2}; *Ezh2*$^{fx/fx}$ mice. We treated mice with the BBN carcinogen and waited 3 months for MIBC onset and progression. After 3 months, mice were assigned to two groups, one receiving corn oil (control) and the other group receiving tamoxifen to acutely induce *Ezh2* deletion in KRT5 (keratin 5)–expressing cells (fig. S1, A and B). At the end point of the experiment, mice from the two groups were euthanized and the bladders were isolated and examined histologically (Fig. 1C). Hematoxylin and eosin staining of the tumors revealed a significant (Fisher's exact test, $P < 0.0001$) reduction of high-stage (T2 or greater) MIBC in the tamoxifen-treated group compared to the control group (Fig. 1C). *Ezh2* deletion in KRT5-expressing cells also induces a hair loss phenotype potentially underlying an important role for EZH2 in regulating hair follicle homeostasis as previously reported (fig. S1C) (*28*). This supports an important role for EZH2 in promoting tumor progression in a carcinogen-induced MIBC mouse model.

To further investigate the role of PRC2 (polycomb repressive complex 2) in this model, we used an EZH2 catalytic inhibitor (EPZ0011989; hereafter EZH2i) to determine whether PRC2 catalytic function was important for tumor development. The experimental approach was similar to the one described above (Fig. 1C); after 3 months of BBN exposure, mice were evaluated for the presence of tumors by magnetic resonance imaging and assigned to a control (vehicle) or a treatment (EZH2i) group. The two groups were treated by twice daily oral gavage for 24 days and euthanized 30 days after treatment (Fig. 1D). Similar to the results obtained with our genetic approach, EZH2 catalytic inhibition led to a significant decrease in the number of high-stage tumors (T2 or greater) compared to control (Fisher's exact test, $P < 0.0001$; Fig. 1D) and a decrease in H3K27me3 levels (fig. S1D).

Tumors arising from BBN treatment are often characterized by a shift to a basal subtype (typical of MIBC) with increased expression of basal markers such as KRT5 and KRT14 (*24*, *29*). Transcriptional analysis of bladders isolated from mice treated with EZH2i compared to vehicle control revealed increased transcriptional levels of luminal markers and decreased levels of basal markers (Fig. 1E). These data support the hypothesis that EZH2 catalytic inhibition in the BBN carcinogen model can significantly reduce tumor progression and induce a reconversion of the molecular subtype in the bladder to low-grade tumors or normal urothelium.

EZH2 catalytic inhibition induces an immune response

When evaluating the pathology of mice treated with EZH2i, in addition to reduced stage (Fig. 1D), we also observed increased immune cell infiltrate into the bladder along with the appearance of tertiary lymphoid structures (TLSs) (Fig. 2A). These TLSs were present in 7 of 12 mice treated with EZH2i compared to 2 of 9 in vehicle-treated mice. In addition, immunocytochemistry analysis showed a significant increase in the number of tumor-infiltrating CD3$^+$ cells in the EZH2i-treated group compared to the vehicle control group ($P = 0.0095$) (Fig. 2, B and C). Flow cytometry analyses of the tumors treated with EZH2i compared to vehicle control confirmed an increased in CD3$^+$ cells in the first group; however, we did not detect any specific changes in the population of T cells infiltrating the tumors (Fig. 2D). This result was also confirmed in our conditional knockout model where *Ezh2*-deleted tumors showed an increased number of CD3$^+$-infiltrating cells compared to *Ezh2* wild-type (WT) tumors (fig. S1E).

Next, we analyzed RNA sequencing (RNA-seq) data to identify transcriptional changes that could provide an explanation for the increased immune infiltration observed in EZH2i-treated BBN tumors. Given the transcriptional repressive activity associated with PRC2 function, we focused our analysis on genes potentially derepressed (activated) upon EZH2 catalytic inhibition compared to control. Gene set enrichment analysis (GSEA) showed that genes with immunoregulatory functions were up-regulated in the EZH2i treatment group relative to the control group, while genes associated with cell cycle progression and DNA repair were down-regulated in this group (Fig. 2E).

Analysis of publicly available TCGA (The Cancer Genome Atlas) (*29*) transcriptomic data for MIBC tumors showed an inverse correlation between *EZH2* levels and levels of transcripts associated with immune regulation. Overall, EZH2 low tumors had a significantly higher immune score and significantly higher levels of CD4$^+$ T cells by multiple immune deconvolution algorithms (Fig. 2F). To determine whether the expression of immune activating cytokines and pathways could be a direct consequence of exposure of BCa cells to EZH2i, we treated two BCa cell lines with EZH2i or vehicle [dimethyl sulfoxide (DMSO)]. Treatment of BCa cell lines with EZH2i leads to increased levels of *CXCL10* and *TNF* compared to the levels detected in cells treated with DMSO (Fig. 3A). We further confirmed that cells treated with EZH2i had significantly increased secretion of CXCL10 (CXC motif chemokine ligand 10) compared to vehicle-treated cells (Fig. 3B). Chromatin immunoprecipitation followed by sequencing for H3K27me3 in both BCa cell lines revealed that *CXCL10* and *TNF* were PRC2 targets supporting a direct transcriptional control by the complex at these loci (Fig. 3C). Global transcriptomic analyses identified significant overall changes in both cell lines and confirmed the enhanced levels of the immune-related genes in cells treated with EZH2i compared to vehicle-treated cells (Fig. 3D). Together, these data support a crucial role for EZH2 in promoting immune suppression in MIBC.

EZH2 controls MHC class II gene expression in BCa cells

Recently, major histocompatibility complex (MHC) class I genes have been identified as a PRC2 target (*30*). Transcriptomic analysis of tumors from the carcinogen-induced MIBC mouse model did not show any difference in terms of MHC class I gene levels in the two groups analyzed (EZH2i versus control; fig. S3A). Nonetheless, we did observe significantly increased levels of MHC class II genes along with a strong increase in the levels of *Ciita*, a master regulator of MHC class II genes expression, in tumors belonging to the EZH2i-treated group compared to control (Fig. 4A and fig. S2A). While MHC class I is present on most nucleated cells, MHC class II expression is restricted to specialized antigen-presenting cells (APCs) (*31*). Therefore, we were interested to explore whether treatment with EZH2i was sufficient to induce expression of APC-restricted markers on epithelial cancer cells. Consistent with our in vivo data, treatment of four BCa cell lines with EZH2i led to a significant increase in the transcript levels of MHC class II genes along with *CIITA* compared to vehicle control (Fig. 4B and fig. S3A). As previously reported in other cells (*32*), *CIITA* locus in BCa cells was marked by PRC2-deposited H3K27me3 (Fig. 4C). In addition, we also observed H3K27me3 marking gene bodies of other MHC class II genes (Fig. 4C). We further confirmed that EZH2i led to decreased H3K27me3 levels at

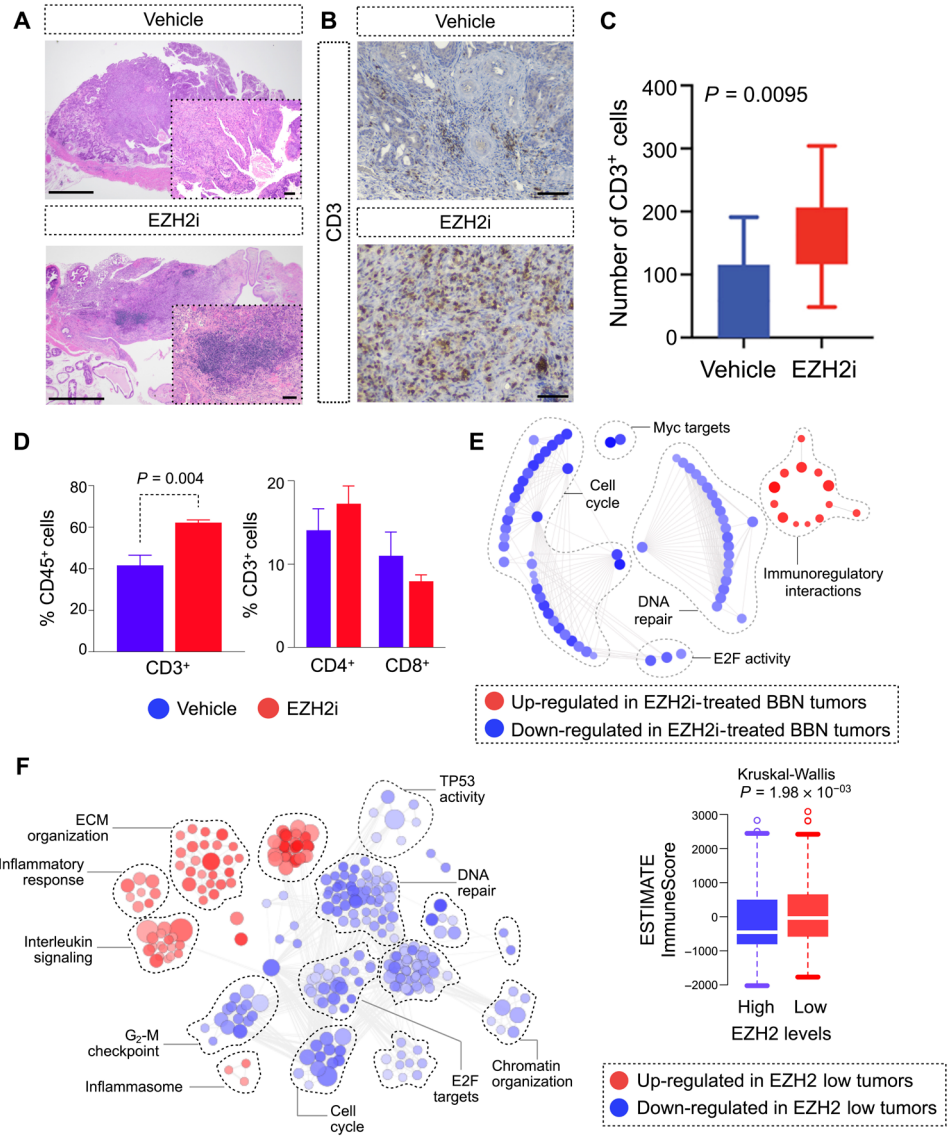

Fig. 2. Immune activation by EZH2. (**A**) Representative hematoxylin and eosin (H&E)–stained sections of BBN tumors from mice treated with EZH2i with tertiary lymphoid structure highlighted on inset. Scale bars, 1 mm (whole bladder) and 100 μm (highlighted inset). (**B** and **C**) Immunohistochemistry images (B) and quantification (C) of $CD3^+$ cells from vehicle control– or EZH2i-treated tumors. Scale bars, 100 μm. (**D**) Flow cytometry analysis of bladders isolated from the EZH2i-treated and vehicle control groups. $CD45^+CD3^+$ T cells and $CD3^+CD4^+/CD3^+CD8^+$ percentages of specific parental populations are represented. There is no statistical difference between $CD3^+CD4^+/CD3^+CD8^+$ distribution in the two groups. (**E**) Network of molecular pathways enriched in each group (EZH2i and vehicle) from RNA sequencing experiments conducted on bladders isolated from the two groups ($n = 6$ EZH2i group and $n = 5$ vehicle group). (**F**) Network of molecular pathways enriched in The Cancer Genome Atlas MIBC cohort segregated based on *EZH2* expression. Inset shows boxplot comparing ESTIMATE immune scores for each group. ECM, extracellular matrix.

the *HLA-DRA* locus (a MHC class II gene) while leading to increased H3K27ac levels when compared to vehicle control, consistent with the *HLA-DRA* enhanced levels in EZH2i versus control (Fig. 4D). We also verified the increased protein levels of MHC class II by Western blotting and detected significantly increased surface levels of MHC class II in BCa cells treated with EZH2i compared to control (Fig. 4E). We further confirmed the implication of PRC2 catalytic activity in the regulation of MHC class II levels by ectopically expressing the histone mutant H3.3K27M or H3.3 WT in BCa cells. According to the general inhibitory activity toward H3K27me3 deposition by the H3.3K27M (*17*), MHC class II protein levels ectopically expressing the histone mutant were increased compared to cells transduced with H3.3 WT or untreated cells, an increase that was comparable to the same induced by the treatment with EZH2i (Fig. 4F). These data strongly support a role for EZH2 and PRC2 catalytic activity in the direct transcriptional regulation of MHC class II levels in BCa cells.

EZH2i effect on UCa progression is entirely dependent on an intact adaptive immune system

To further confirm our in vitro findings in vivo, we decided to use a transgenic mouse model that can express the ovalbumin (OVA) antigen on the surface of the urothelium (*33*). These mice were exposed to the BBN carcinogen and divided into two groups after 14 days,

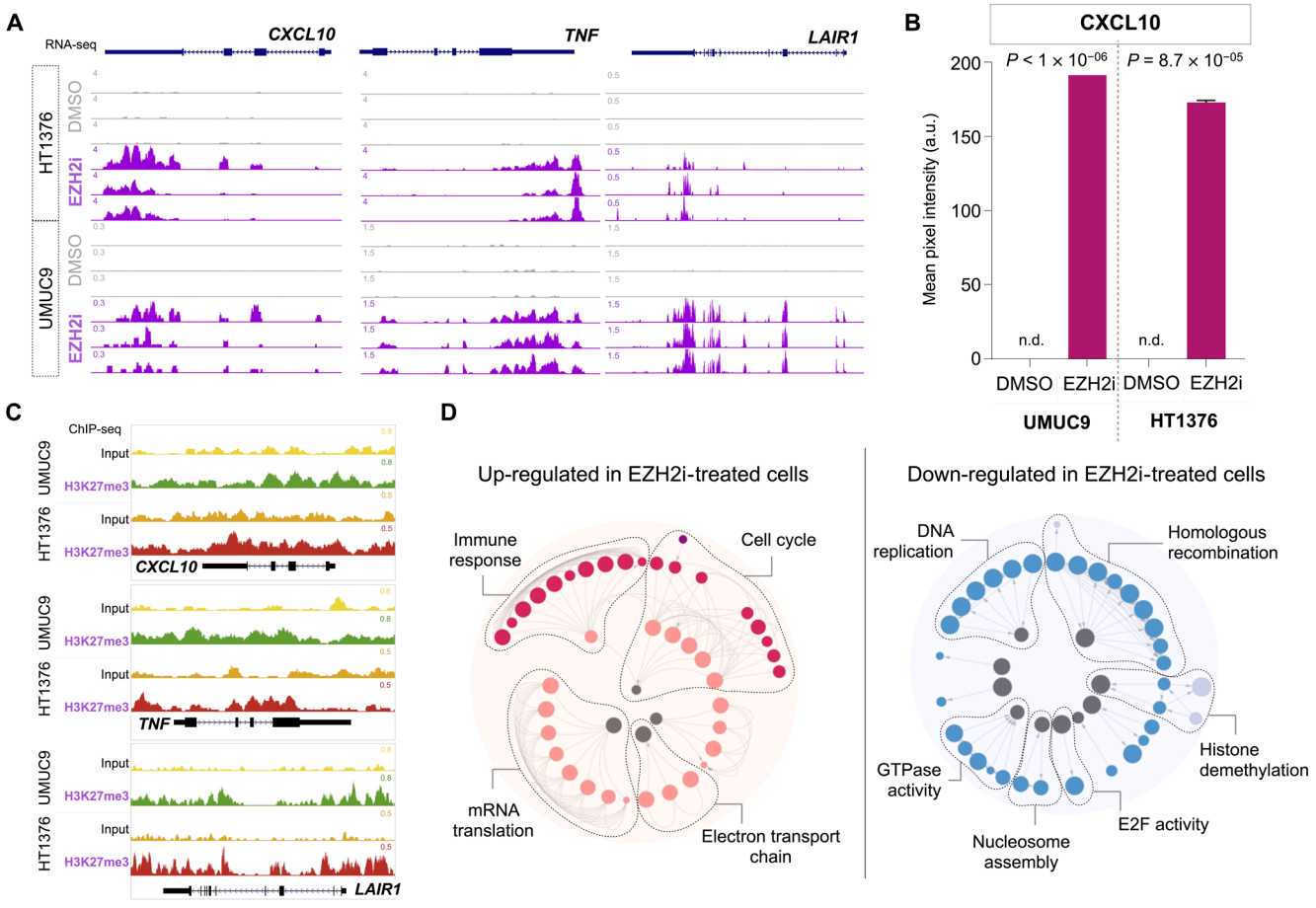

Fig. 3. Treatment with EZH2i up-regulates markers of immunogenicity and increases infiltration of immune cells into bladder tumors. (**A**) Transcriptomic changes in BCa cell lines (HT1376 and UMUC9) treated with EZH2i mirrored changes observed in murine tumors treated with the drug with significant up-regulation of immune signaling pathways. RNA-seq, RNA sequencing. (**B**) Cytokine profiling in supernatant from BCa cell lines HT1376 and UMUC9 revealed strong concordance between cytokine production and transcriptomic changes after treatment with EZH2i. a.u., arbitrary units; n.d., not determined. (**C**) H3K27me3 chromatin immunoprecipitation sequencing (ChIP-seq) reveals increased H3K27me3 signal around loci of immune genes [CXCL10, TNF (tumor necrosis factor), and LAIR1 (Leukocyte Associated Immunoglobulin Like Receptor 1)] in BCa cell lines (UMUC9 and HT1376). (**D**) Networks depicting GSEA results from comparison of UMUC9 and HT1376 cells treated with EZH2i or DMSO control. GTPase, guanosine triphosphatase.

one treated with EZH2i and the other with vehicle control. After 14 days of treatment (total 28 days of BBN exposure), cells were isolated from bladders obtained from the two groups (EZH2i and vehicle control). Bladder cells from each of the two groups were cocultured with T cells ($CD8^+$ or $CD4^+$) derived from transgenic mice bearing T cell receptors (TCRs) specific against the OVA antigen (OTI and OTII)[3] (Fig. 5A). In the coculture experiment, interferon-γ (IFN-γ) and interleukin-17 (IL-17) release was measured as an indication of T cell activation mediated by the interaction OVA-TCRs. When bladder cells were cultured in the absence of T cells, very minimal levels of secreted IFN-γ and IL-17 were detected, with no significant difference between the EZH2i group and the control group (Fig. 5B). However, $CD8^+$ (OT-I) or $CD4^+$ (OT-II) T cells cocultured with bladder cells from the EZH2i-treated group showed significantly increased levels of both IFN-γ and IL-17 compared to the control group (Fig. 5B). Flow cytometry analyses of tumor masses reveal increased levels of infiltrating innate immune cells in mice treated with EZH2i compared to control (fig. S4A). These cells might be participating to the increased T cell–mediated response that we observed in EZH2i-treated compared to vehicle-treated mice. These data support a strong T cell activation toward tumors treated with EZH2i compared to tumors treated with vehicle control.

On the basis of these data and the transcriptional activation of immune cytokines in BCa tumors from mice treated with EZH2i compared to control group, we hypothesized that the activity of tumor-infiltrating T cells could, at least in part, contribute to the reduced tumor progression observed in EZH2i-treated mice. To test this hypothesis, we reproduced the carcinogen-induced MIBC model in immunocompromised mice with deletion of the adaptive immune system. We administered the BBN carcinogen to *Rag1*$^{-/-}$ mice that have a targeted deletion of the recombinase necessary for lymphocyte development (*34*). Mice were administered with BBN for 3 months followed by 24 days of treatment with EZH2i or vehicle control (Fig. 5C). In contrast to what we observed in WT mice, we found an opposite effect in tumor stage, *Rag1*$^{-/-}$, mice after treatment with EZH2i or vehicle control. Mice treated with EZH2i show a significant increase number of higher stage tumors compared to mice treated with vehicle control (Figs. 1D and 5D). These data formally prove that adaptive immunocompetence is crucial for the antitumor activity of EZH2i in a carcinogen-induced MIBC mouse model.

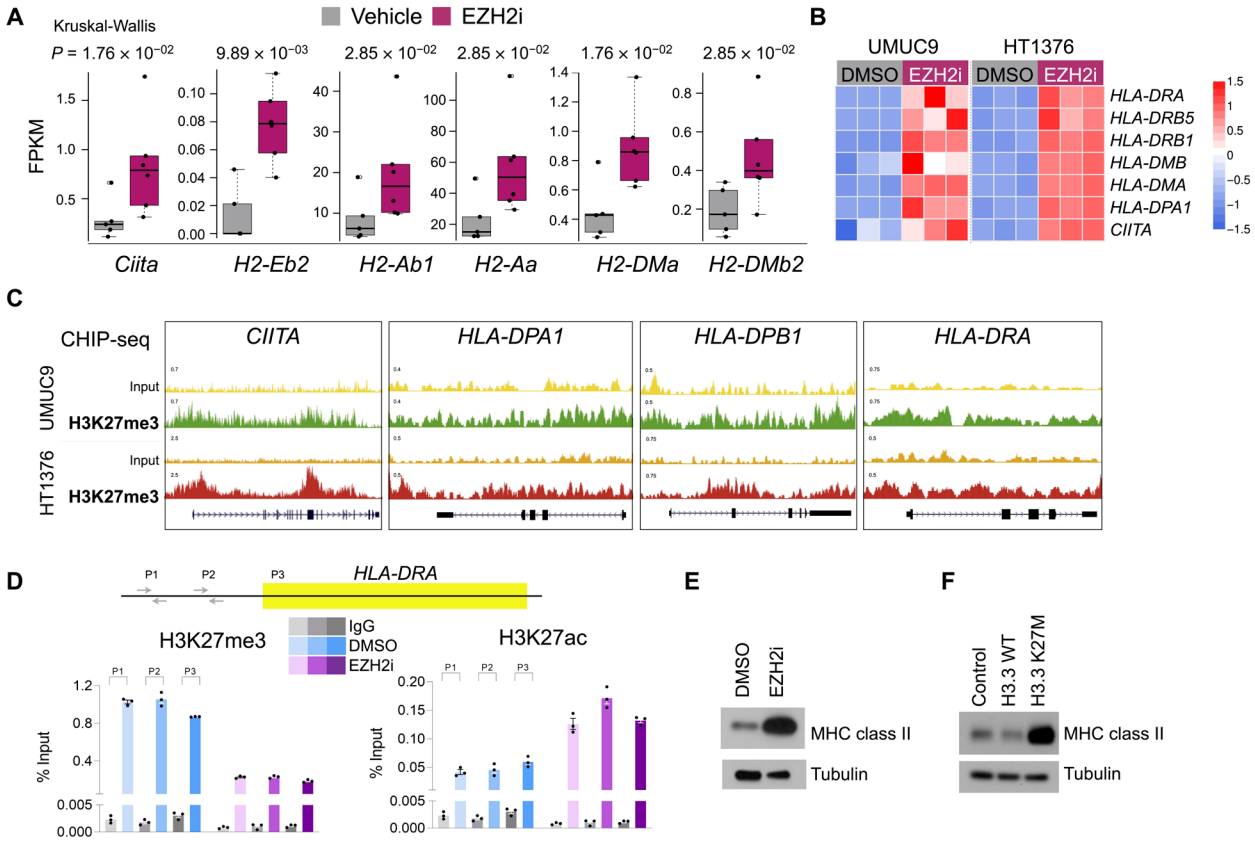

Fig. 4. Treatment with EZH2i reverses PRC2-mediated silencing of MHC class II genes. (**A**) Transcriptomic changes in tumors from mice treated with EZH2i highlighting transcripts with a role in antigen presentation. (**B**) EZH2 inhibition induces expression of MHC class II genes in human BCa cell line (HT1376). (**C**) Increased H3K27me3 signal is detected by ChIP-seq around loci of MHC class II genes in BCa cells. (**D**) ChIP–quantitative polymerase chain reaction for enrichment of H3K27me3/H3K27ac at *HLA-DRA* gene locus in HT1376 cells treated with EZH2i or DMSO. (**E**) MHC class II expression in HT1376 cells treated with EZH2i or DMSO. (**F**) MHC class II expression in HT1376 cells expressing control, H3.3 WT, or H3.3K27M.

DISCUSSION

To date, the pathways associated with cancer immune evasion have largely focused on antigen presentation, recognition by the immune system, and recruitment of immune cells (*3*). Deregulation of *EZH2*, the PRC2 catalytic subunit, has been reported in several types of cancer where it generally has a pro-oncogenic function (*20*). The pro-oncogenic role of *EZH2* has been investigated in BCa cells and in xenograft mouse models where *EZH2* was shown to favor tumor proliferation through a cell autonomous mechanism (*23*). PRC2 and *EZH2* dysregulation in cancer is generally regarded to promote tumorigenesis in a cell autonomous manner (*35*). To the best of our knowledge, very few studies have reported a non–cell autonomous pro-oncogenic function of *EZH2* (*30*, *36*). To date, there are no studies in a carcinogen-induced animal tumor model that have evaluated the immunomodulatory impact of EZH2 inhibition in tumor progression through a non–cell autonomous mechanism. Taking advantage of a mouse model of UCa that recapitulates the genetic and pathologic complexity of the analogous human disease, including an intact immune system (*24*), we evaluated the role of *Ezh2* in MIBC. Although EZH2 catalytic inhibition was never tested in a carcinogen-induced UCa mouse model, previous studies have suggested the potential efficacy of this therapeutic strategy (*23*). In our model, we observed a drastic reduction in tumor progression in mice treated with EZH2 catalytic inhibitor compared to control. We also observed a basal-to-luminal shift in the transcriptional program supporting the less aggressive histologic analysis (Fig. 1). These data are compatible with the classical role of *EZH2* in maintaining malignant proliferation in a cell autonomous manner (*37*); however, we did not anticipate a significant involvement of the immune system that we observed in mice treated with EZH2i. In tumors that responded to EZH2i treatment, there was a significant increase in tumor-infiltrating $CD3^+$ T cells and a clear enrichment of an immune-activating transcriptional signature compared to vehicle-treated tumors (Fig. 2). Using BCa cell lines, we were able to recapitulate the activation of immunoregulatory pathways upon EZH2i treatment compared to control treatment (Fig. 3). This supported the idea that cancer epithelial cells, after EZH2i treatment, were increasing/inducing the transcriptional and protein levels of genes involved in immune response pathways including the potent CXCL10 cytokine that is known to attract immune cells such as T cells (*38*) and is directly targeted by the PRC2-deposited H3K27me3 (Fig. 3) (*39*). Of clinical interest, high levels of CXCL10 have been associated with an improved response to immunotherapy in metastatic BCa (*40*). In addition, both in BCa cell lines and in the carcinogen-induced BBN mouse model, we were able to show that several transcripts and proteins involved in MHC class II antigen presentation were strongly increased in cells/tumors treated with EZH2i compared to control and were direct PRC2 targets (Fig. 4). This prompted an

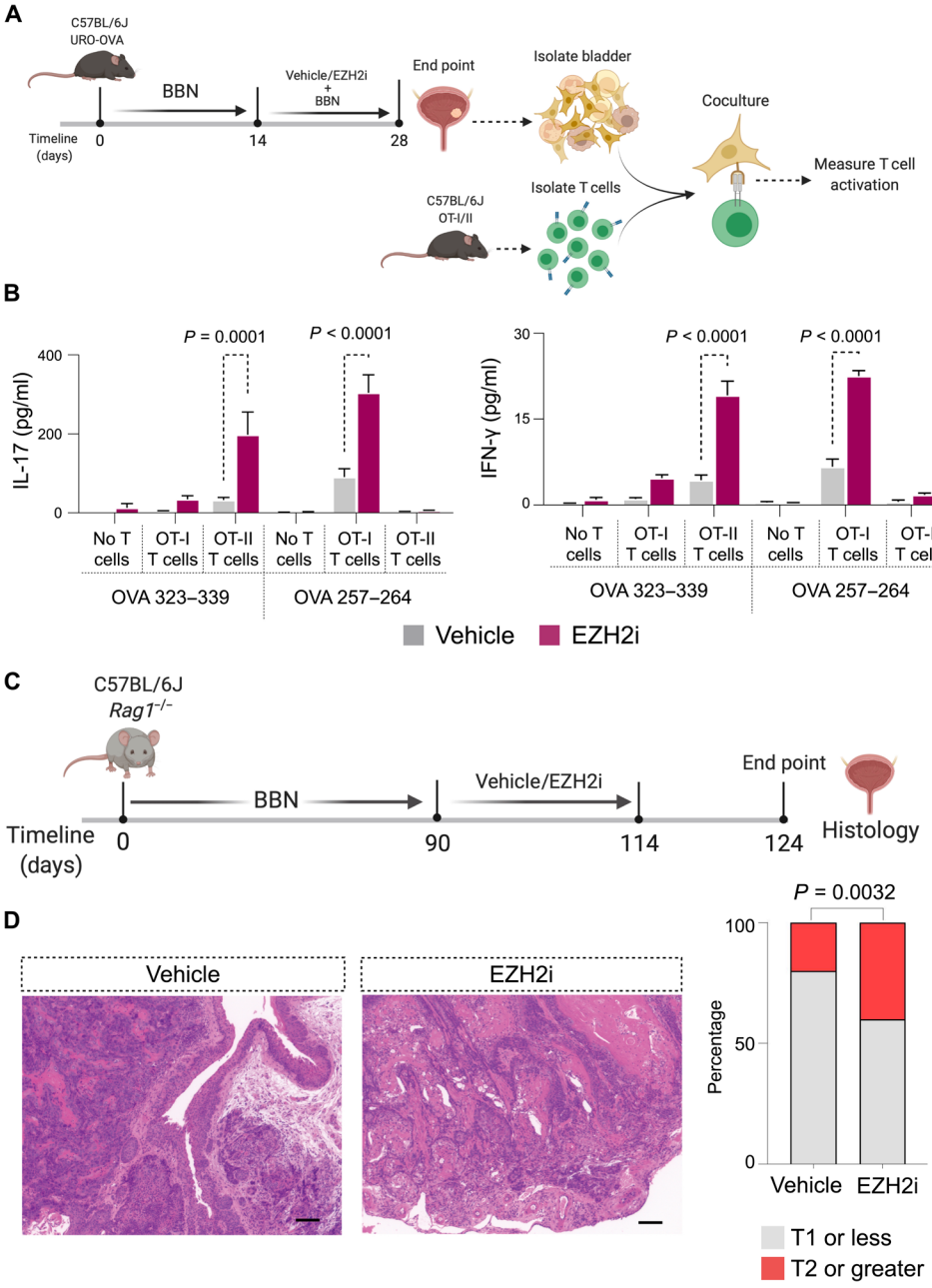

Fig. 5. A functional adaptive immune system is required for response to EZH2i. (**A** and **B**) Schematic for experiment designed to evaluate role of $CD4^-$ MHC class II interaction in EZH2i-induced antitumor immunity. (**B**) Interleukin-17 (IL-17) and interferon-γ (IFN-γ) cytokine levels in indicated experimental conditions. (**C** and **D**) Male *Rag1*$^{-/-}$ C57BL/6 mice received water containing 0.05% BBN for 90 days, after which mice were treated with vehicle control or EZH2i for 24 days. (C) Schematic of experimental design to evaluate the role of the adaptive immune system in observed response to EZH2i in carcinogen-induced tumor model. (D) Representative H&E-stained sections of BBN tumors from *Rag1*$^{-/-}$ mice treated with vehicle control or EZH2i. Similar aggressive morphology was observed in both groups. Scale bars, 100μm.

investigation into the role played by the adaptive immune system in our model upon EZH2 catalytic inhibition. We hypothesized that the involvement of the immune system was secondary to an increased cytokine and chemokine production as well as an increased MHC class II antigen presentation, as we observed increased cytokine, chemokine, and MHC class II genes levels in BCa cell lines and murine tumors treated with EZH2i compared to control. Using the URO-OVA system, we showed that EZH2 inhibition can induce a non–cell autonomous T cell response against tumors cells derived from BBN-induced BCas (Fig. 5). These data strongly support a non–cell autonomous role for EZH2 in BCa cells to promote tumor progression in the BBN-induced MIBC model through the activation and recruitment of adaptive immune system toward the tumor.

PRC2 has been previously demonstrated to partially affect immune response in melanoma and ovarian cancer (*41*, *42*). Notably, in our model, and distinct from previous studies, the entire antitumor progression effect achieved through Ezh2 catalytic inhibition is fully dependent on an intact adaptive immune system. Carcinogen-induced

MIBC in immunodeficient (*Rag1*$^{-/-}$) mice were insensitive to EZH2 catalytic inhibition, and we even show a statistically increased number of higher-stage tumors compared to the control group (Fig. 5). This result might be explained by a non–cell autonomous mechanism of action of the inhibitor potentially promoting innate immune cells functions in the absence of a functional adaptive immune system (*43*). This will be an intriguing line of investigation for future studies. Together, our results support a crucial role for EZH2 in maintaining low immunogenicity of BCa cells by transcriptionally repressing cytokines and MHC class II antigen presentation genes. Our data also open to the intriguing hypothesis that EZH2 catalytic inhibition might stimulate BCa cells to present tumor antigens in an MHC class II–restricted manner, although this would need to be carefully tested experimentally. On the basis of the results from this research, a clinical trial has been initiated to evaluate the efficacy of tazemetostat (EZH2 catalytic inhibitor) and pembrolizumab (PD1 inhibitor) in treating patients with locally advanced or metastatic UCa (NCT03854474) (*44*). Our study demonstrates a non–cell autonomous function of PRC2 catalytic activity in promoting the progression of MIBC through immune evasion in a carcinogen-induced mouse model.

MATERIALS AND METHODS

Mice and tumor staging

Mice were cared for as per recommendations from the Animal Care and Use Committee (IS00004049 and IS00008422) at Northwestern University. All research was approved by an animal research protocol and carried out using procedures described previously (*45*). Briefly, 6-week-old male C57BL/6 mice were fed BBN at a dose of 0.05% in drinking water ad libitum for 12 weeks, after which mice were randomized to receive either EPZ011989 or vehicle. Mice were gavaged twice daily, at a dose of 500 mg/kg, for 5 days a week with a 2-day break on a 7-day cycle. At the end of treatment, animals were euthanized by CO_2 with secondary cervical dislocation. Bladders were removed and divided in the sagittal plane and either fixed in 10% formalin or snap-frozen in liquid nitrogen. Tumor stage was determined using human AJCC (American Joint Committee on Cancer) staging on the basis of the depth of bladder wall invasion. Mice URO-OVA used in the manuscript have a C57Bl/6:SJL background (*33*).

RNA extraction, library generation, and sequencing

RNA extraction from mouse tumors was performed as described previously (*45*). Briefly, mouse tumors were ground using liquid nitrogen and mortar and pestle. Next, RNA was extracted using TRIZol reagent (Thermo Fisher Scientific) following the manufacturer's instructions. RNA quality and concentration were measured by NanoDrop and then Qubit Fluorometric Quantitation (Thermo Fisher Scientific). Library preparation and RNA-seq were performed at the NuSeq core facility (Northwestern University) using an Illumina HiSeq 2000. Fastq files were processed using Ceto pipeline created by E. Bartom. Briefly, RNA-seq reads were aligned to mm10 reference genome using STAR (v 2.7.5). Gene expression was quantified using HTSeq, and differential gene expression profiles were generated using DESeq2. To identify differentially expressed gene programs comparing the two groups, a $\log_2$ fold change ranked list was generated. Next ranked genes were used as input for GSEA (version 4.1.0). Resulting enrichment was visualized using the Enrichment map (*46*) (version 3.3.3) plugin within Cytoscape (version 3.9.0). Results were exported and further analyzed in R.

Cytokine array experiments

UMUC9 and HT1376 cell lines were seeded at a concentration of 10,000 cells/ml in a 6-cm culture dish. Cells were treated with DMSO or EPZ011989 at a concentration of 5 μM for 7 days. Media were replaced with fresh media containing drug every other day. On day 7, 500 μl of supernatant was taken for each condition and analyzed for cytokines with the Proteome Profiler Human Cytokine array kit (R&D Systems, catalog no. ARY005B).

Transcriptomic analysis (cell lines)

UMUC3, UMUC9, HT1376, and 5637 (American Type Culture Collection) cell lines were treated with DMSO or EPZ011989 at a concentration of 5 μM for 7 days. Media were replaced with fresh media containing drug every other day. On day 7, cells were harvested for RNA extraction. RNA was extracted using QIAGEN RNeasy kit according to the manufacturer's instructions. Libraries were prepared according to manufacturer's protocol and sequenced on the NextSeq 500 or NovaSeq 6000 (Illumina). Fastq files were processed using Ceto pipeline created by E. Bartom. Briefly, RNA sequence reads were aligned to hg38 reference genome using STAR (v 2.7.5). Gene expression was quantified using HTSeq and differential gene expression profiles were generated using DESeq2. Next, a $\log_2$ fold change ranked list was generated. Ranked genes were used as input for GSEA. Resulting enrichment was visualized using the Enrichment map plugin within Cytoscape.

TCGA analysis

RNA-seq data for muscle invasive bladder tumors in TCGA (*29*) cohort were downloaded using TCGAbiolinks R package (*47*). HTSeq counts were used as input into DESeq2 to generate differential gene expression profiles which were further analyzed using GSEA and Enrichment app to generate expression networks. Tumors were classified into high- or low-EZH2 expressing based on EZH2 fpkm values. For immune deconvolution, immunedeconv (*48*–*52*) R package was used and tumors were grouped into two groups based on the top and bottom 25% EZH2-expressing tumors.

Immunohistochemistry

Immunohistochemistry procedure was performed as described previously (*45*). Briefly, bladders were fixed in 10% formalin and embedded in paraffin. Sections (4 μm) were used for CD8 (1:1000; Invitrogen, #MA5-13263) and Foxp3 (1:400; Cell Signaling Technology, #12653) staining. Dako Autostainer Plus instrument (Dako, CO, USA) and anti-rabbit Dako EnVision+ System-HRP (horseradish peroxidase) (Dako) were used. For each tumor, HRP-positive cells were counted in the 10× objective field. At least two separate sections and six different fields were evaluated for each tumor.

Flow cytometry (cell lines)

UMUC9 and HT1376 cell lines were treated with DMSO or EPZ011989 at a concentration of 5 μM for 7 days. Media were replaced with fresh media containing drug every other day. On day 7, cells were harvested and processed for analysis of surface expression of MHC class II by flow cytometry. Approximately 10,000 cells were analyzed per sample. Cells were stained with fluorescein isothiocyanate (FITC) mouse anti-human HLA-DR antibody (BD Biosciences, 556643) or FITC rat IgG2α (immunoglobulin G2α), κ isotype control (BD Biosciences, 553929) and analyzed using BD LSRFortessa.

Flow cytometry

Analysis of immune cell populations was performed as described previously (*45*). Briefly, spleens were dissociated into a single-cell suspension followed by red blood cell lysis. For the bladder, single-cell suspensions were prepared by mincing the bladder tissue in 2 ml of Accutase (MilliPore) plus collagenase (1 mg/ml) at 37°C for 30 min. Following enzymatic digestion, bladder samples were strained through a 100-μm cell strainer, and the strainer was washed twice with 10 ml of Hanks' balanced salt solution + 5% fetal calf serum, and the cells were pelleted. Next, cells were washed in phosphate-buffered saline, stained with LIVE/DEAD Fixable Aqua Dead Cell Stain (Life Technologies; Grand Island, NY), blocked with anti-CD16/32 (Thermo Fisher Scientific), followed by antibody staining. A total of 10^6 viable cells were analyzed per individual sample using a BD LSRFortessa (BD Bioscience), and the data were analyzed using the FlowJo version 9.5.2 software (Tree Star Inc., Ashland, OR).

Coculture of isolated bladder cells with OTI and OTII T cells

For coculture of cells isolated from the bladder with either OTI or OTII T Cells, $CD8^+$ T cells and $CD4^+$ T cells were magnetically sort purified (EasySep) from the spleens of male OTI and OTII TCR transgenic mice (Jackson Laboratory). Total bladder cells were isolated from URO-OVA mice that had received BBN for 4 weeks and either vehicle or EZHi treatment for 2 weeks before bladder collection using the same tissue digestion method listed above. Cells (isolated cells from the bladder cells and T cells) within the cocultures were age- and gender-matched. Bladder cells (1×10^5 cells per well) and T cells (2×10^5 cells per well) were cultured in the presence of media only (negative control), OVA-257, or OVA-353 peptide (Genemed Synthesis) (20 μg/ml). Culture supernatants were collected on day 5 of culture, and the level of cytokine was measured via the Luminex High Sensitivity Mouse T Cell Cytokine Assay Kit (Milliplex).

Statistical analysis

Comparisons of the percentage of animals showing clinical disease were analyzed by χ^2 using Fisher's exact probability test, and statistical tests used to generate *P* values are highlighted in the figures. For most of the analysis described here, R version 4.0.3 or GraphPad Prism version 9.3.1 was used to analyze the data and generate the figures.

SUPPLEMENTARY MATERIALS

Supplementary material for this article is available at https://science.org/doi/10.1126/sciadv.abo8043

View/request a protocol for this paper from *Bio-protocol*.

REFERENCES AND NOTES

1. R. L. Siegel, K. D. Miller, H. E. Fuchs, A. Jemal, Cancer statistics, 2021. *CA Cancer J. Clin.* **71**, 7–33 (2021).
2. A. M. Kamat, R. Li, M. A. O'Donnell, P. C. Black, M. Roupret, J. W. Catto, E. Comperat, M. A. Ingersoll, W. P. Witjes, D. J. McConkey, J. A. Witjes, Predicting response to intravesical bacillus Calmette-Guérin immunotherapy: Are we there yet? A systematic review. *Eur. Urol.* **73**, 738–748 (2018).
3. P. L. Crispen, S. Kusmartsev, Mechanisms of immune evasion in bladder cancer. *Cancer Immunol. Immunother.* **69**, 3–14 (2020).
4. T. J. Curiel, Tregs and rethinking cancer immunotherapy. *J. Clin. Invest.* **117**, 1167–1174 (2007).
5. L. Dyrskjøt, M. A. Ingersoll, Biology of nonmuscle-invasive bladder cancer. *Curr. Opin. Urol.* **28**, 598–603 (2018).
6. S. S. Chang, S. A. Boorjian, R. Chou, P. E. Clark, S. Daneshmand, B. R. Konety, R. Pruthi, D. Z. Quale, C. R. Ritch, J. D. Seigne, E. C. Skinner, N. D. Smith, J. M. McKiernan, Diagnosis and treatment of non-muscle invasive bladder cancer: AUA/SUO Guideline. *J. Urol.* **196**, 1021–1029 (2016).
7. C. Biot, C. A. Rentsch, J. R. Gsponer, F. D. Birkhäuser, H. Jusforgues-Saklani, F. Lemaître, C. Auriau, A. Bachmann, P. Bousso, C. Demangel, L. Peduto, G. N. Thalmann, M. L. Albert, Preexisting BCG-specific T cells improve intravesical immunotherapy for bladder cancer. *Sci. Transl. Med.* **4**, 137ra172 (2012).
8. A. C. Antonelli, A. Binyamin, T. M. Hohl, M. S. Glickman, G. Redelman-Sidi, Bacterial immunotherapy for cancer induces CD4-dependent tumor-specific immunity through tumor-intrinsic interferon-γ signaling. *Proc. Natl. Acad. Sci. U.S.A.* **117**, 18627–18637 (2020).
9. C. A. Rentsch, F. D. Birkhäuser, C. Biot, J. R. Gsponer, A. Bisiaux, C. Wetterauer, M. Lagranderie, G. Marchal, M. Orgeur, C. Bouchier, A. Bachmann, M. A. Ingersoll, R. Brosch, M. L. Albert, G. N. Thalmann, Bacillus calmette-guérin strain differences have an impact on clinical outcome in bladder cancer immunotherapy. *Eur. Urol.* **66**, 677–688 (2014).
10. J. L. Boormans, R. De Wit, G. S. Kulkarni, E. M. Uchio, M. Roumiguié, L. E. M. Krieger, E. A. Singer, D. F. Bajorin, A. M. Kamat, P. Grivas, H. K. Seo, H. Nishiyama, B. R. Konethy, T. Saretsky, H. Li, K. Nam, E. Kapadia, A. V. Balar, Updated follow-up from KEYNOTE-057: Phase 2 study of pembrolizumab (pembro) for patients (pts) with high-risk (HR) non–muscle invasive bladder cancer (NMIBC) unresponsive to bacillus Calmette-Guérin (BCG). *Eur. Urol. Open Sci.* **19**, e1173–e1174 (2020).
11. J. Bellmunt, R. de Wit, D. J. Vaughn, Y. Fradet, J.-L. Lee, L. Fong, N. J. Vogelzang, M. A. Climent, D. P. Petrylak, T. K. Choueiri, A. Necchi, W. Gerritsen, H. Gurney, D. I. Quinn, S. Culine, C. N. Sternberg, Y. Mai, C. H. Poehlein, R. F. Perini, D. F. Bajorin; KEYNOTE-045 Investigators, Pembrolizumab as second-line therapy for advanced urothelial carcinoma. *N. Engl. J. Med.* **376**, 1015–1026 (2017).
12. A. V. Balar, D. Castellano, P. H. O'Donnell, P. Grivas, J. Vuky, T. Powles, E. R. Plimack, N. M. Hahn, R. de Wit, L. Pang, M. J. Savage, R. F. Perini, S. M. Keefe, D. Bajorin, J. Bellmunt, First-line pembrolizumab in cisplatin-ineligible patients with locally advanced and unresectable or metastatic urothelial cancer (KEYNOTE-052): A multicentre, single-arm, phase 2 study. *Lancet Oncol.* **18**, 1483–1492 (2017).
13. M. D. Galsky, J. Á. A. Arija, A. Bamias, I. D. Davis, M. De Santis, E. Kikuchi, X. Garcia-del-Muro, U. De Giorgi, M. Mencinger, K. Izumi, S. Panni, M. Gumus, M. Özgüroğlu, A. R. Kalebasty, S. H. Park, B. Alekseev, F. A. Schutz, J. R. Li, D. Ye, N. J. Vogelzang, S. Bernhard, D. Tayama, S. Mariathasan, A. Mecke, A. C. Thåström, E. Grande, Atezolizumab with or without chemotherapy in metastatic urothelial cancer (IMvigor130): A multicentre, randomised, placebo-controlled phase 3 trial. *Lancet* **395**, 1547–1557 (2020).
14. A. G. Robertson, C. S. Groeneveld, B. Jordan, X. Lin, K. A. McLaughlin, A. Das, L. A. Fall, D. Fantini, T. J. Taxter, L. S. Mogil, S. V. Lindskrog, L. Dyrskjøt, D. J. McConkey, R. S. Svatek, A. de Reyniès, M. A. A. Castro, J. J. Meeks, Identification of differential tumor subtypes of T1 bladder cancer. *Eur. Urol.* **78**, 533–537 (2020).
15. S. Hinz, C. Kempkensteffen, F. Christoph, M. Hoffmann, H. Krause, M. Schrader, M. Schostak, K. Miller, S. Weikert, Expression of the polycomb group protein EZH2 and its relation to outcome in patients with urothelial carcinoma of the bladder. *J. Cancer Res. Clin. Oncol.* **134**, 331–336 (2008).
16. H. Wang, R. Albadine, A. Magheli, T. J. Guzzo, M. W. Ball, S. Hinz, M. P. Schoenberg, G. J. Netto, M. L. Gonzalgo, Increased EZH2 protein expression is associated with invasive urothelial carcinoma of the bladder. *Urol. Oncol.* **30**, 428–433 (2012).
17. A. Piunti, A. Shilatifard, The roles of Polycomb repressive complexes in mammalian development and cancer. *Nat. Rev. Mol. Cell Biol.* **22**, 326–345 (2021).
18. A. Piunti, A. Shilatifard, Epigenetic balance of gene expression by Polycomb and COMPASS families. *Science* **352**, aad9780 (2016).
19. A. Piunti, D. Pasini, Epigenetic factors in cancer development: Polycomb group proteins. *Future Med.* **7**, 57–75 (2011).
20. K. H. Kim, C. W. M. Roberts, Targeting EZH2 in cancer. *Nat. Med.* **22**, 128–134 (2016).
21. A. Piunti, A. Rossi, A. Cerutti, M. Albert, S. Jammula, A. Scelfo, L. Cedrone, G. Fragola, L. Olsson, H. Koseki, G. Testa, S. Casola, K. Helin, F. D. A. Di Fagagna, D. Pasini, Polycomb proteins control proliferation and transformation independently of cell cycle checkpoints by regulating DNA replication. *Nat. Commun.* **5**, 1–14 (2014).
22. D. Hanahan, R. A. Weinberg, Hallmarks of cancer: The next generation. *Cell* **144**, 646–674 (2011).
23. L. D. Ler, S. Ghosh, X. Chai, A. A. Thike, H. L. Heng, E. Y. Siew, S. Dey, L. K. Koh, J. Q. Lim, W. K. Lim, S. S. Myint, J. L. Loh, P. Ong, X. X. Sam, D. Huang, T. Lim, P. P. H. Tan, S. Nagarajan, C. W. S. Cheng, H. Ho, L. G. Ng, J. Yuen, P. H. Lin, C. K. Chuang, Y. H. Chang, W. H. Weng, S. G. Rozen, P. P. H. Tan, C. L. Creasy, S. T. Pang, M. T. Mccabe, S. L. Poon, B. T. Teh, Loss of tumor suppressor KDM6A amplifies PRC2-regulated transcriptional repression in bladder cancer and can be targeted through inhibition of EZH2. *Sci. Transl. Med.* **9**, eaai8312 (2017).
24. D. Fantini, A. P. Glaser, K. J. Rimar, Y. Wang, M. Schipma, N. Varghese, A. Rademaker, A. Behdad, A. Yellapa, Y. Yu, C. C. Sze, L. Wang, Z. Zhao, S. E. Crawford, D. Hu, J. D. Licht, C. K. Collings, E. Bartom, D. Theodorescu, A. Shilatifard, J. J. Meeks, A carcinogen-induced mouse model recapitulates the molecular alterations of human muscle invasive bladder cancer. *Oncogene* **37**, 1911–1925 (2018).
25. M. Santos, M. Martínez-Fernández, M. Dueñas, R. García-Escudero, B. Alfaya, F. Villacampa, C. Saiz-Ladera, C. Costa, M. Oteo, J. Duarte, V. Martínez, M. J. Gómez-Rodriguez,

M. L. Martín, M. Fernández, P. Viatour, M. A. Morcillo, J. Sage, D. Castellano, J. L. Rodriguez-Peralto, F. De La Rosa, J. M. Paramio, In vivo disruption of an Rb–E2F–Ezh2 signaling loop causes bladder cancer. *Cancer Res.* **74**, 6565–6577 (2014).
26. A. P. Glaser, D. Procissi, Y. Yu, J. J. Meeks, Magnetic resonance imaging assessment of carcinogen-induced murine bladder tumors. *J. Vis. Exp.* 10.3791/59101 (2019).
27. K. Shin, A. Lim, J. I. Odegaard, J. D. Honeycutt, S. Kawano, M. H. Hsieh, P. A. Beachy, Cellular origin of bladder neoplasia and tissue dynamics of its progression to invasive carcinoma. *Nat. Cell Biol.* **16**, 469–478 (2014).
28. E. Ezhkova, W. H. Lien, N. Stokes, H. A. Pasolli, J. M. Silva, E. Fuchs, EZH1 and EZH2 cogovern histone H3K27 trimethylation and are essential for hair follicle homeostasis and wound repair. *Genes Dev.* **25**, 485–498 (2011).
29. A. G. Robertson, J. Kim, H. Al-Ahmadie, J. Bellmunt, G. Guo, A. D. Cherniack, T. Hinoue, P. W. Laird, K. A. Hoadley, R. Akbani, M. A. A. Castro, E. A. Gibb, R. S. Kanchi, D. A. Gordenin, S. A. Shukla, F. Sanchez-Vega, D. E. Hansel, B. A. Czerniak, V. E. Reuter, X. Su, B. D. S. Carvalho, V. S. Chagas, K. L. Mungall, S. Sadeghi, C. S. Pedamallu, Y. Lu, L. J. Klimczak, J. Zhang, C. Choo, A. I. Ojesina, S. Bullman, K. M. Leraas, T. M. Lichtenberg, C. J. Wu, N. Schultz, G. Getz, M. Meyerson, G. B. Mills, D. J. McConkey, J. N. Weinstein, D. J. Kwiatkowski, S. P. Lerner, R. Akbani, H. Al-Ahmadie, M. Albert, I. Alexopoulou, A. Ally, T. Antic, M. Aron, M. Balasundaram, J. Bartlett, S. B. Baylin, A. Beaver, J. Bellmunt, I. Birol, L. Boice, M. S. Bootwalla, J. Bowen, R. Bowlby, D. Brooks, B. M. Broom, W. Bshara, S. Bullman, E. Burks, F. M. Cárcano, R. Carlsen, B. S. Carvalho, A. L. Carvalho, E. P. Castle, M. A. A. Castro, P. Castro, J. W. Catto, V. S. Chagas, A. D. Cherniack, D. W. Chesla, C. Choo, E. Chuah, S. Chudamani, V. K. Cortessis, S. L. Cottingham, D. Crain, E. Curley, B. A. Czerniak, S. Daneshmand, J. A. Demchok, N. Dhalla, H. Djaladat, J. Eckman, S. C. Egea, J. Engel, I. Felau, M. L. Ferguson, J. Gardner, J. M. Gastier-Foster, M. Gerken, G. Getz, E. A. Gibb, C. R. Gomez-Fernandez, D. A. Gordenin, G. Guo, D. E. Hansel, J. Harr, A. Hartmann, L. M. Herbert, T. Hinoue, T. H. Ho, K. A. Hoadley, R. A. Holt, C. M. Hutter, S. J. M. Jones, M. Jorda, R. J. Kahnoski, R. S. Kanchi, K. Kasaian, J. Kim, L. J. Klimczak, D. J. Kwiatkowski, P. H. Lai, P. W. Laird, B. R. Lane, K. M. Leraas, S. P. Lerner, T. M. Lichtenberg, J. Liu, L. Lolla, Y. Lotan, Y. Lu, F. R. Lucchesi, Y. Ma, R. D. Machado, D. T. Maglinte, D. Mallery, M. A. Marra, S. E. Martin, M. Mayo, D. J. McConkey, A. Meraney, M. Meyerson, G. B. Mills, A. Moinzadeh, R. A. Moore, E. M. M. Pinero, S. Morris, C. Morrison, K. L. Mungall, A. J. Mungall, J. B. Myers, R. Naresh, P. H. O'Donnell, A. I. Ojesina, D. J. Parekh, J. Parfitt, J. D. Paulauskis, C. S. Pedamallu, R. J. Penny, T. Pihl, S. Porten, M. E. Quintero-Aguilo, N. C. Ramirez, W. K. Rathmell, V. E. Reuter, K. Rieger-Christ, A. G. Robertson, S. Sadeghi, C. Saller, A. Salner, F. Sanchez-Vega, G. Sandusky, C. Scapulatempo-Neto, J. E. Schein, A. K. Schuckman, N. Schultz, C. Shelton, T. Shelton, S. A. Shukla, J. Simko, P. Singh, P. Sipahimalani, N. D. Smith, H. J. Sofia, A. Sorcini, M. L. Stanton, G. D. Steinberg, R. Stoehr, X. Su, T. Sullivan, Q. Sun, A. Tam, R. Tarnuzzer, K. Tarvin, H. Taubert, N. Thiessen, L. Thorne, K. Tse, K. Tucker, D. J. Van Den Berg, K. E. Van Kessel, S. Wach, Y. Wan, Z. Wang, J. N. Weinstein, D. J. Weisenberger, L. Wise, T. Wong, Y. Wu, C. J. Wu, L. Yang, L. A. Zach, J. C. Zenklusen, J. Zhang, J. Zhang, E. Zmuda, E. C. Zwarthoff, Comprehensive molecular characterization of muscle-invasive bladder cancer. *Cell* **171**, 540–556.e25 (2017).
30. M. L. Burr, C. E. Sparbier, K. L. Chan, Y.-C. C. Chan, A. Kersbergen, E. Y. N. Lam, E. Azidis-Yates, D. Vassiliadis, C. C. Bell, O. Gilan, S. Jackson, L. Tan, S. Q. Wong, S. Hollizeck, E. M. Michalak, H. V. Siddle, M. T. McCabe, R. K. Prinjha, G. R. Guerra, B. J. Solomon, S. Sandhu, S.-J. J. Dawson, P. A. Beavis, R. W. Tothill, C. Cullinane, P. J. Lehner, K. D. Sutherland, M. A. Dawson, An evolutionarily conserved function of polycomb silences the MHC class I antigen presentation pathway and enables immune evasion in cancer. *Cancer Cell* **36**, 385–401.e8 (2019).
31. M. L. Axelrod, R. S. Cook, D. B. Johnson, J. M. Balko, Biological consequences of MHC-II expression by tumor cells in cancer. *Clin. Cancer Res.* **25**, 2392–2402 (2019).
32. N. T. Mehta, A. D. Truax, N. H. Boyd, S. F. Greer, Early epigenetic events regulate the adaptive immune response gene CIITA. *Epigenetics* **6**, 516–525 (2011).
33. W. Liu, D. P. Evanoff, X. Chen, Y. Luo, Urinary bladder epithelium antigen induces $CD8^+$ T cell tolerance, activation, and autoimmune response. *J. Immunol.* **178**, 539–546 (2007).
34. P. Mombaerts, J. Iacomini, R. S. Johnson, K. Herrup, S. Tonegawa, V. E. Papaioannou, RAG-1-deficient mice have no mature B and T lymphocytes. *Cell* **68**, 869–877 (1992).
35. A. Laugesen, J. W. Højfeldt, K. Helin, Role of the polycomb repressive complex 2 (PRC2) in transcriptional regulation and cancer. *Cold Spring Harb. Perspect. Med.* **6**, a026575 (2016).
36. S. Ramakrishnan, V. Granger, M. Rak, Q. Hu, K. Attwood, L. Aquila, N. Krishnan, R. Osiecki, G. Azabdaftari, K. Guru, G. Chatta, G. Gueron, L. McNally, J. Ohm, J. Wang, A. Woloszynska, Inhibition of EZH2 induces NK cell-mediated differentiation and death in muscle-invasive bladder cancer. *Cell Death Differ.* **26**, 2100–2114 (2019).
37. S. H. Tang, H. S. Huang, H. U. Wu, Y. T. Tsai, M. J. Chuang, C. P. Yu, S. M. Huang, G. H. Sun, S. Y. Chang, P. W. Hsiao, D. S. Yu, T. L. Cha, Pharmacologic down-regulation of EZH2 suppresses bladder cancer in vitro and in vivo. *Oncotarget* **5**, 10342–10355 (2014).
38. J. H. Dufour, M. Dziejman, M. T. Liu, J. H. Leung, T. E. Lane, A. D. Luster, IFN-γ-inducible protein 10 (IP-10; CXCL10)-deficient mice reveal a role for IP-10 in effector T cell generation and trafficking. *J. Immunol.* **168**, 3195–3204 (2002).
39. N. Nagarsheth, D. Peng, I. Kryczek, K. Wu, W. Li, E. Zhao, L. Zhao, S. Wei, T. Frankel, L. Vatan, W. Szeliga, Y. Dou, S. Owens, V. Marquez, K. Tao, E. Huang, G. Wang, W. Zou, PRC2 epigenetically silences Th1-type chemokines to suppress effector T-cell trafficking in colon cancer. *Cancer Res.* **76**, 275–282 (2016).
40. J. E. Rosenberg, J. Hoffman-Censits, T. Powles, M. S. Van Der Heijden, A. V. Balar, A. Necchi, N. Dawson, P. H. O'Donnell, A. Balmanoukian, Y. Loriot, S. Srinivas, M. M. Retz, P. Grivas, R. W. Joseph, M. D. Galsky, M. T. Fleming, D. P. Petrylak, J. L. Perez-Gracia, H. A. Burris, D. Castellano, C. Canil, J. Bellmunt, D. Bajorin, D. Nickles, R. Bourgon, G. M. Frampton, N. Cui, S. Mariathasan, O. Abidoye, G. D. Fine, R. Dreicer, Atezolizumab in patients with locally advanced and metastatic urothelial carcinoma who have progressed following treatment with platinum-based chemotherapy: A single-arm, multicentre, phase 2 trial. *Lancet* **387**, 1909–1920 (2016).
41. D. Zingg, N. Arenas-Ramirez, J. Haeusel, L. Sommer, O. Boyman, The histone methyltransferase Ezh2 controls mechanisms of adaptive resistance to tumor immunotherapy. *Cell Rep.* **20**, 854–867 (2017).
42. D. Peng, I. Kryczek, N. Nagarsheth, L. Zhao, S. Wei, W. Wang, Y. Sun, E. Zhao, L. Vatan, W. Szeliga, J. Kotarski, R. Tarkowski, Y. Dou, K. Cho, S. Hensley-Alford, A. Munkarah, R. Liu, W. Zou, Epigenetic silencing of TH1-type chemokines shapes tumour immunity and immunotherapy. *Nature* **527**, 249–253 (2015).
43. S. Mola, G. Pinton, M. Erreni, M. Corazzari, M. De Andrea, A. A. Grolla, V. Martini, L. Moro, C. Porta, Inhibition of the histone methyltransferase EZH2 enhances protumor monocyte recruitment in human mesothelioma spheroids. *Int. J. Mol. Sci.* **22**, 4391 (2021).
44. ClinicalTrials.gov, *Tazemetostat and Pembrolizumab in Treating Patients With Locally Advanced or Metastatic Urothelial Carcinoma* (ClinicalTrials.gov).
45. J. R. Podojil, A. P. Glaser, D. Baker, E. T. Courtois, D. Fantini, Y. Yu, V. Eaton, S. Sivajothi, M. Chiang, A. Das, K. A. McLaughlin, P. Robson, S. D. Miller, J. J. Meeks, Antibody targeting of B7-H4 enhances the immune response in urothelial carcinoma. *Onco. Targets. Ther.* **9**, 1744897 (2020).
46. J. Reimand, R. Isserlin, V. Voisin, M. Kucera, C. Tannus-Lopes, A. Rostamianfar, L. Wadi, M. Meyer, J. Wong, C. Xu, D. Merico, G. D. Bader, Pathway enrichment analysis and visualization of omics data using g: Profiler, GSEA, cytoscape and enrichmentMap. *Nat. Protoc.* **14**, 482–517 (2019).
47. A. Colaprico, T. C. Silva, C. Olsen, L. Garofano, C. Cava, D. Garolini, T. S. Sabedot, T. M. Malta, S. M. Pagnotta, I. Castiglioni, M. Ceccarelli, G. Bontempi, H. Noushmehr, TCGAbiolinks: An R/Bioconductor package for integrative analysis of TCGA data. *Nucleic Acids Res.* **44**, e71 (2016).
48. B. Li, E. Severson, J.-C. Pignon, H. Zhao, T. Li, J. Novak, P. Jiang, H. Shen, J. C. Aster, S. Rodig, S. Signoretti, J. S. Liu, X. S. Liu, Comprehensive analyses of tumor immunity: Implications for cancer immunotherapy. *Genome Biol.* **17**, 174 (2016).
49. G. Sturm, F. Finotello, F. Petitprez, J. D. Zhang, J. Baumbach, W. H. Fridman, M. List, T. Aneichyk, Comprehensive evaluation of transcriptome-based cell-type quantification methods for immuno-oncology. *Bioinformatics* **35**, i436–i445 (2019).
50. A. M. Newman, C. L. Liu, M. R. Green, A. J. Gentles, W. Feng, Y. Xu, C. D. Hoang, M. Diehn, A. A. Alizadeh, Robust enumeration of cell subsets from tissue expression profiles. *Nat. Methods* **12**, 453–457 (2015).
51. J. Racle, K. De Jonge, P. Baumgaertner, D. E. Speiser, D. Gfeller, Simultaneous enumeration of cancer and immune cell types from bulk tumor gene expression data. *eLife* **6**, e26476 (2017).
52. D. Aran, Z. Hu, A. J. Butte, xCell: Digitally portraying the tissue cellular heterogeneity landscape. *Genome Biol.* **18**, 220 (2017).

Acknowledgments: We thank M. Morgan for providing us with the H3.3 WT and H3.3 K27M plasmids. We thank A. Das and A. Glaser for technical expertise. **Funding:** J.J.M. is supported by grants from the VHA BX003692 and BX005599. A.P. was supported by the transition to independence grant K99CA234434. **Author contributions:** Conceptualization: A.P., J.J.M., A.S., and S.D.M. Methodology: A.P., K.M., Y.Y., A.G.R., J.R.P., K.A.M., Z.Y., D.F., M.C., Y.L., L.W., N.H., J.Q., S.D.M., A.S., and J.J.M. Investigation: A.P., K.M., Y.Y., A.G.R., J.R.P., K.A.M., Z.Y., D.F., M.C., Y.L., L.W., N.H., J.Q., S.D.M., A.S., and J.J.M. Visualization: K.M., A.G.R., J.R.P., K.A.M., and D.F. Supervision: A.P., A.G.R., Y.L., S.D.M., A.S., and J.J.M. Writing—original draft, review, and editing: A.P., K.M., Y.Y., A.G.R., J.R.P., K.A.M., Z.Y., D.F., M.C., Y.L., L.W., N.H., J.Q., S.D.M., A.S., and J.J.M. **Competing interests:** J.J.M. received reagent (EPZ011989) from Epizyme Inc. and limited research funds for specimen analysis. A.P. is a shareholder of Epizyme Inc. D.F. is an employee of Xilio Therapeutics and a former employee and a stockholder of Eli Lilly and Company. The other authors declare that they have no other competing interests. **Data and materials availability:** All data needed to evaluate the conclusions in the paper are present in the paper and/or the Supplementary Materials. All sequencing data have been deposited to GEO under the accession ID GSE209853. EPZ011989 was provided by Epizyme Inc. under a material transfer agreement. Requests for EPZ011989 should be submitted to M. J. Hinrichs at mary.jane.hinrichs@ipsen.com

Submitted 27 February 2022
Accepted 17 August 2022
Published 5 October 2022
10.1126/sciadv.abo8043